Review of Palaeobotany and Palynology 334 (2025) 105270

Contents lists available at ScienceDirect

Review of Palaeobotany and Palynology

journal homepage: www.elsevier.com/locate/revpalbo

New palynological data and U–Pb dating from the Jiufotang Formation: Implications for the late Jehol Biota

Qiaoer Ying [a,b], Shouliang Sun [c,*], Duojia Zhang [d], Fei Liang [a,b,*], Yuhui Feng [a,b], Guodong Wang [a,b], Shiying Wang [a,b], Eugenia Bugdaeva [e], Valentina Markevich [e], Mihai Emilian Popa [f]

[a] College of Palaeontology, Shenyang Normal University, Shenyang 110034, China
[b] Key-Lab of Evolution of Past Life in NE Asia, Ministry of Natural Resources, Shenyang 110034, China
[c] Shenyang Center of Geological Survey, China Geological Survey, Shenyang 110034, Liaoning, China
[d] China University of Geosciences, 430074 Wuhan, Hubei, China.
[e] Federal Scientific Center of East Asia Terrestrial Biodiversity, FEB RAS, Vladivostok 690022, Russia
[f] University of Bucharest, Faculty of Geology and Geophysics, Department of Geology and Doctoral School of Geology, Laboratory of Palaeontology, Bucharest, Romania

ARTICLE INFO

Keywords:
Palynology
Zircon dating
Aptian
Jiufotang Formation

ABSTRACT

The Lower Cretaceous terrestrial strata of northeast China are predominantly located in northern Hebei, western Liaoning, Jilin, and eastern Inner Mongolia Provinces. Among these, the Jiufotang Formation in western Liaoning has garnered significant global attention due to its rich fossil record, particularly in relation to Jehol Biota. The age of the Jiufotang Formation has long been debated primarily due to the absence of biostratigraphic fossil evidence. In this study, we analyzed the palynological content collected from the Jiufotang Formation in the Pijiagou section of the Fuxin Basin. A total of 41 species in 24 palynomorph genera were recognized as belonging to the *Appendicisporites-Pinuspollenites-Jiaohepollis* assemblage. We documented the new occurrence of *Appendicisporites imperfectus* in the Jiufotang Formation, which has been recognized as a valid biostratigraphic indicator for Aptian palynological assemblages, thereby providing crucial new palynological evidence for dating this formation. Furthermore, LA-ICP-MS zircon U–Pb dating for a rhyolitic tuff yielded a new age of 118.07 ± 0.98 Ma, suggesting that the Pijiagou section was dated to the middle Aptian. Based on the palynological data, the Lower Cretaceous Jiufotang flora was represented by coniferous forests. Considering the associated biota, the palaeoenvironment during the middle Aptian was characterized by a sub-humid warm temperate climate with seasonal changes.

1. Introduction

The Cretaceous strata are widespread and varied in China, and the Lower Cretaceous terrestrial strata in northeastern China mainly occur within volcanic sedimentary basins distributed in northern Hebei, western Liaoning, and eastern Inner Mongolia Provinces (Wan et al., 2007; Xi et al., 2019). The Fuxin Basin of western Liaoning Province was one of the main coal- and oil-bearing basins in northeast China during the Mesozoic Era, and its Cretaceous strata, including the Yixian, Jiufotang, Shahai, Fuxin, and Sunjiawan formations are well developed (Chen and Jin, 1999; Zhou et al., 2003; Sha, 2007; Wu et al., 2015; Xi et al., 2019). The strata of the Jiufotang Formation in western Liaoning are well developed and rich in terrestrial organism fossils from various taxa, including the world famous Jehol Biota, with evidence for the origin and early evolution of birds, insects, and angiosperms (Ji et al., 2004; Zhou, 2014; Zhou and Wang, 2017; Wu et al., 2018; Xu et al., 2020). However, its age is still debated due to the scarcity of available biostratigraphic fossils and dating data from the Jiufotang Formation (He et al., 2004; Chang et al., 2009; Yu et al., 2021). In recent years, radiometric dating data of the tuff layers in the Jiufotang Formation have ranged from 122.1 to 118.9 Ma, corresponding to the late Barremian to the Aptian (He et al., 2004; Chang et al., 2009; Yu et al., 2021). Previous dates for the Jiufotang Formation were obtained from different locations, e.g., the Chaoyang – Beipiao and Jianchang Basins (Chang et al., 2009; Yu et al., 2021). Isotope chronology is scarce in the Fuxin Basin; thus, radiometric dating of the tuff layers is still necessary in the

* Corresponding authors.
E-mail addresses: sunsolar@qq.com (S. Sun), liangfei5777@163.com (F. Liang).

https://doi.org/10.1016/j.revpalbo.2024.105270
Received 20 August 2024; Received in revised form 4 December 2024; Accepted 9 December 2024
Available online 12 December 2024

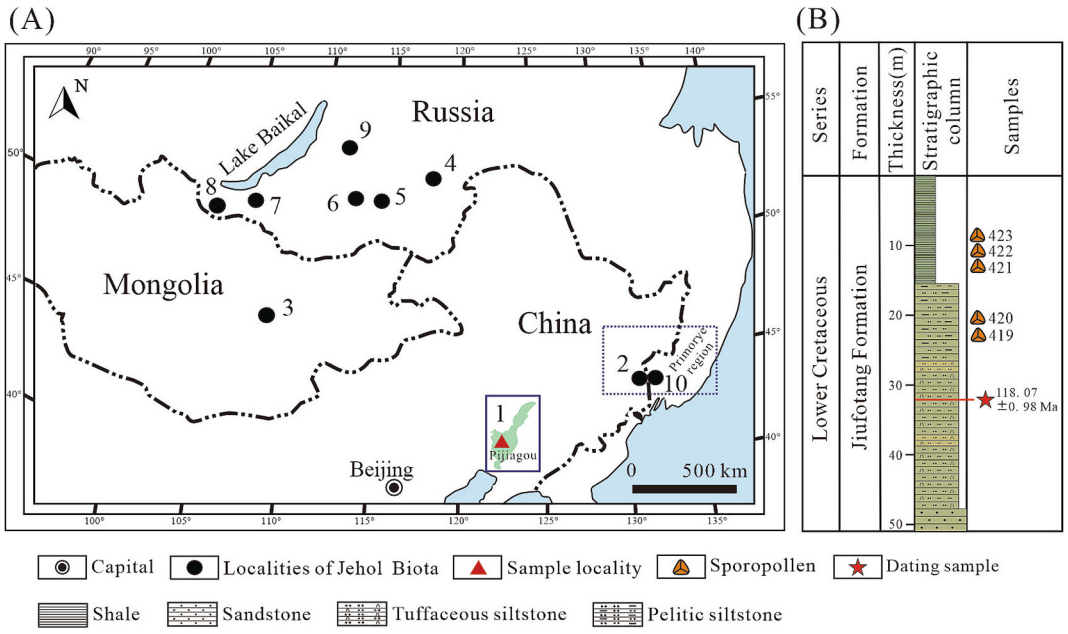

Fig. 1. Occurrence and stratigraphic column of the Jiufotang Formation.
A. Location of the Jiufotang Formation in the Fuxin Basin and locations of the Jehol Biota in Russia and Mongolia (revised from Bugdaeva and Golovneva, 2024), 1. Pijiagou section, Fuxin Basin of western Liaoning Province, China; 2. Dongning Formation of Heilongjiang Province, northeast China; 3. Tevshiin Govi Formation, Tevshiin Govi Coal Mine, Mongolia; 4. Turga Formation, Bukachacha Basin of Eastern Transbaikalia, Russia; 5. Turga Formation of Semion locality, Central Transbaikalia, Russia; 6. Turga Formation, Chita–Ingoda Basin, Central Transbaikalia, Russia; 7. Selenga Formation, Gusinoe Ozero Basin, western Transbaikalia, Russia; 8. Sanga Formation of Khasurty locality, western Transbaikalia, Russia; 9. Zaza Formation of Baisa locality, Central Transbaikalia, Russia; 10. Lipovtsy Formation, Razdolnaya River Basin, Russia. Chinese base map from the Standard Map Service, plan approval number: GS (2022) 4302. B. The composite stratigraphic column and all sampling horizons of the Jiufotang Formation in the Fuxin Basin.

Jiufotang Formation. The fossiliferous layers of the Jiufotang Formation provide evidence for biostratigraphical correlations, including birds, plants, fossil wood, and palynomorphs (Pu and Wu, 1985; Yu et al., 1986; Zhou, 2014; Wang et al., 2015; Wang et al., 2020), although the available biostratigraphic fossils associated with these correlations have yet to be clearly defined.

In this study, we present U–Pb zircon dating data from the Jiufotang Formation in the Fuxin Basin that was obtained using the LA-ICP-MS method. These data serve as supplementary evidence for stratigraphic correlations. Additionally, the new palynological data offer valuable insights into palaeoenvironmental and palaeoclimate reconstructions related to the Jiufotang Formation in the Fuxin Basin.

2. Geological setting

The Fuxin Basin, one of the typical faulted basins in western Liaoning Province (Wu et al., 2015), is distributed in the northern part of the North China Plate and northeastern part of the Yanshan Tectonic Belt (Wang et al., 1998; Zhang et al., 2005). The Jiufotang Formation in western Liaoning Province is widely distributed, mainly developed in Fuxin, Jianchang, and Chaoyang – Beipiao Basins (Su et al., 2008). The Pijiagou section, located in the south – central part of the Fuxin Basin, mainly exposed the upper part of the Jiufotang Formation (Fig. 1A, Chen et al., 2019). This section is dominated by shore-shallow lake deposits and yielded vertebrate remains such as *Confuciusornis* (*Jinzhouonzis*), *Yixianomis*, *Microraptor*, *Ikechosaurus* and *Hyphalosaurus*, along with abundant well-preserved ostracods (Zhang et al., 2007). All samples of this study were collected from the Jiufotang Formation in the Pijiagou section of the Fuxin Basin (Fig. 1A–B).

3. Material and methods

All radiometric dating and palynomorph samples were collected from the Lower Cretaceous Jiufotang Formation in the Fuxin Basin, western Liaoning Province, northeast China (Fig. 1A). The rhyolitic tuff samples were collected for dating (sampling horizons were marked in Fig. 1B). 20 palynological samples were collected from the Pijiagou section of the Jiufotang Formation, which mainly comprise grayish-yellow tuff siltstone, grayish-yellow sandstone, and light grayish-green shale (Fig. 1B). Only 5 palynological samples contained spores and pollen; their inventory numbers were marked in Fig. 1B (named as 419, 420, 421, 422 and 423 in ascending order). The naming methods for fossils were primarily based on the guidelines established by Song et al. (2000).

3.1. Palynological analysis

All samples were initially pulverized into fine powder. Each sample (20 g) underwent two sequential treatments with HCl (30%) and HF (40%) to remove carbonate and silicate minerals, respectively. During each treatment, the samples were washed multiple times with distilled water. Subsequently, all samples were exposed to a NaOH (5%) solution for one hour. The remaining residues were rinsed with distilled water and then passed through a 10 μm mesh sieve. Slides were mounted using glycerin jelly and sealed with nail polish. At least 200 sporomorphs were counted in each sample. Palynomorphs were identified and counted under Leica DM3000 microscope, and images were photographed using a Leica DMC5400 microscopic imaging system. All palynological samples and mounted slides were stored in the Key Lab of Evolution of Past Life in NE Asia of Paleontology of Liaoning, Shenyang Normal University.

3.2. U–Pb dating

Zircon particles were isolated utilizing heavy liquid and magnetic methods at the Beijing CreaTech Testing Technology Co., Ltd. in Beijing, China. The preferred zircon crystals were then embedded in epoxy resin and carefully polished to expose their internal structure. Transmitted

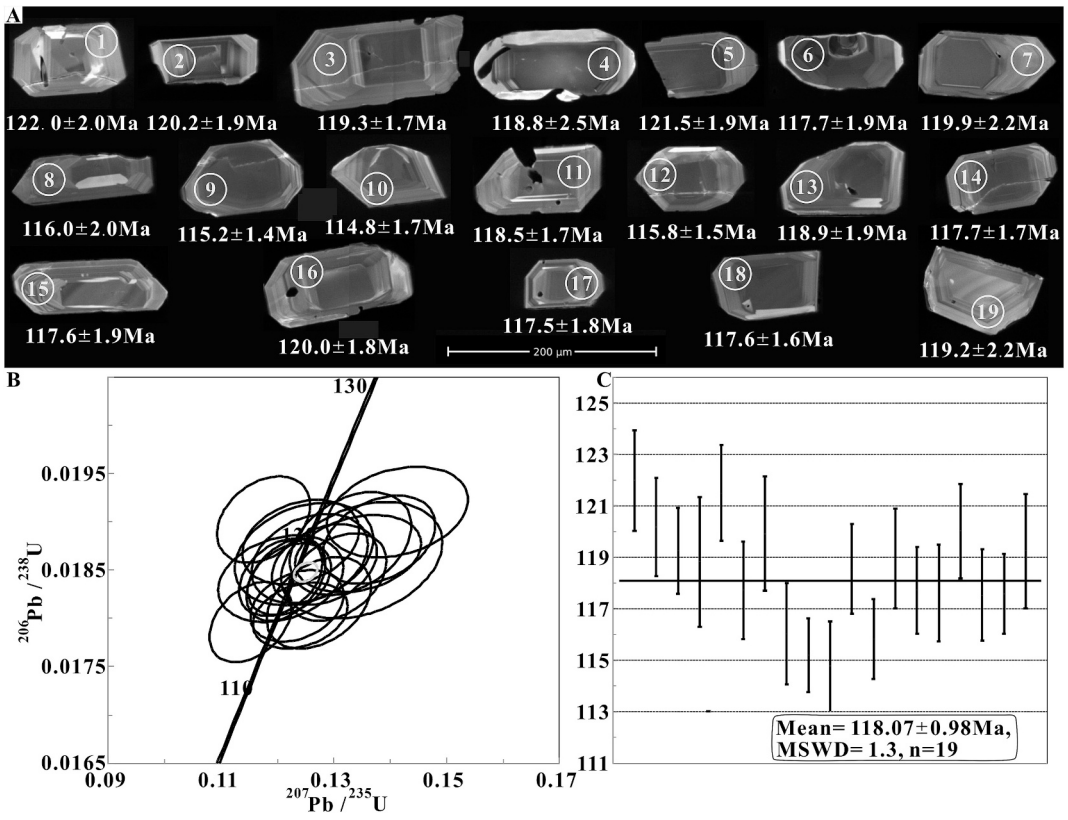

Fig. 2. Illustrations of U–Pb dating analysis and results.
A. CL images; B. Concordia plots of the rhyolitic tuff; C. The weighted mean ages of the rhyolitic tuff.

light, reflected light, and cathodoluminescence (CL) were applied to each zircon crystal to examine details such as microfractures, internal inclusions, and oscillatory zoning, etc., to precisely identify the analysis locations. U–Pb dating analyses were conducted with LA-ICP-MS (Laser ablation-inductively coupled plasma mass spectrometer), conducted in the same company as zircon selection. The analytical setup comprised an AnalytikJena PQMS Elite ICP-MS instrument coupled with a 193-nm excimer laser ablation system (RESOlution). Helium was applied as a carrier gas. Operating with a laser beam diameter of 24 μm, an energy density of 8 J cm^{-2}, and a repetition rate of 6 Hz, the system provided highly accurate results. Each batch of ten samples underwent two analyses using zircon standard GJ-1, one with zircon standard Plesovice, and another with glass standard NIST 610 (Jackson et al., 2004; Hou et al., 2009; Geng et al., 2011). Off-line raw data selection, integration of background, analytical signals, time-drift correction, and quantitative calibration for U–Pb dating were processed using ICPMSDataCal (Liu et al., 2010), while the Concordia diagram and weighted average ages were calculated utilizing Isoplot software (Ludwig, 2003; Liu et al., 2008).

4. Results

4.1. Zircon U–Pb dating

Representative zircon cathodoluminescence images, selected LA spot locations, and spot ages are illustrated in Fig. 2A, while the Concordia plots and weighted mean ages are presented in Fig. 2B–C. Comprehensive data pertaining to Uranium (U) and Thorium (Th) concentrations, isotopic ratios, and the age of each zircon grain are tabulated in Table 1. In the dating process, a total of 25 spots from 25 zircons were scrutinized, with 19 grains exhibiting a discordance of less than 5%. These zircons typically exhibit sub-euhedral to euhedral shapes, ranging from 100 to 300 μm in length, and boasting an aspect ratio varying between 1 and 5. Distinctive oscillatory zoning patterns are observed in the CL images, along with Th/U ratios spanning from 0.44 to 0.75 (Table 1), suggesting a magmatic origin (Koschek, 1993). The dating results of these zircons conform to the Concordia curve, yielding a weighted mean $^{206}Pb/^{238}U$ age of 118.07 ± 0.98 million years (n = 19, MSWD = 1.3), which represents the eruption age of this rhyolitic tuff sample.

4.2. Palynological assemblage

Five palynological samples yield diverse and well-preserved palynomorphs. A total of 41 species in 24 genera of palynomorphs are recognized (Table 2). Based on the presence of certain taxa with stratigraphical significance in palynomorph compositions of the Jiufotang Formation, this assemblage is named the *Appendicisporites-Pinuspollenites-Jiaohepollis* assemblage (APJ assemblage). A prominent characteristic of this assemblage is the dominance of gymnosperm pollen (avg. 98.62%) over fern spores (avg. 1.83%). Among the fern spores, *Cyathidites* (avg. 0.24%; Fig. 3A), *Lycopodiumsporites* (avg. 0.16%; Fig. 3B), *Punctatisporites* (avg. 0.52%; Fig. 3C), *Appendicisporites imperfectus* (avg. 0.1%; Fig. 3D), and *Osmundacidites wellmanii* (avg. 0.34%; Fig. 3E) are the common taxa. The gymnosperm pollen is mainly composed of bisaccate grains, the percentage of *Classopollis* (Cheirolepidiaceae; Fig. 3F–G) is relatively small (avg. 0.75%); the percentage of monosulcate pollen of cycadophytes/ginkgophytes (Fig. 3H) is 1.98% on average, and the pollen with a single sac or no sac is much higher than fern spores, represented by *Araucariacites* (avg. 21.10%; Fig. 3I), *Psophosphaera* (avg. 21.10%; Fig. 3J), *Callialasporites* (avg. 0.68%; Fig. 3K), and *Jiaohepollis* (avg. 0.7%; Fig. 3L). Bisaccate conifer pollen is the most abundant, represented by *Alisporites* (avg. 2.3%; Fig. 3M), *Podocarpidites* (avg. 1.98%; Fig. 3N), *Cedripites* (avg. 3.8%; Fig. 3O), *Piceapollenites* (avg. 12.56%; Fig. 3P), *Piceites* (avg. 0.26%; Fig. 3Q), *Parcisporites* (avg. 0.08%; Fig. 3R), and *Pinuspollenites* (avg. 24.66%; Fig. 3S), suggesting

Table 1
LA-ICP-MS zircon U–Pb data of samples.

Spots No.	Content ($\times 10^{-6}$)		Th/U	Isotope ratios								Age (Ma)						Concordance
	Th	U		$^{207}Pb/^{206}Pb$	1σ	$^{207}Pb/^{235}U$	1σ	$^{206}Pb/^{238}U$	1σ	$^{208}Pb/^{232}Th$	1σ	$^{207}Pb/^{206}Pb$	1σ	$^{207}Pb/^{235}U$	1σ	$^{206}Pb/^{238}U$	1σ	
1	145.0622	222.5289	0.6519	0.0538	0.0032	0.1413	0.0083	0.0191	0.0003	0.0061	0.0002	361.2	133.3	134.2	7.3	122.0	2.0	90%
2	2521.2121	1481.4488	1.7019	0.0536	0.0027	0.1380	0.0066	0.0188	0.0003	0.0063	0.0002	353.8	111.1	131.3	5.9	120.2	1.9	91%
3	147.0314	216.5207	0.6791	0.0522	0.0029	0.1343	0.0074	0.0187	0.0003	0.0060	0.0002	294.5	127.8	128.0	6.6	119.3	1.7	92%
4	408.1223	295.0633	1.3832	0.0531	0.0038	0.1350	0.0094	0.0186	0.0004	0.0056	0.0002	331.5	160.2	128.5	8.4	118.8	2.5	92%
5	228.6857	346.2625	0.6604	0.0476	0.0020	0.1175	0.0054	0.0190	0.0003	0.0064	0.0002	81.2	101.6	112.8	4.9	121.5	1.9	92%
6	308.9739	413.9727	0.7464	0.0514	0.0022	0.1306	0.0058	0.0184	0.0003	0.0057	0.0001	257.5	100.0	124.6	5.2	117.7	1.9	94%
7	1211.3833	1090.7959	1.1105	0.0520	0.0029	0.1330	0.0071	0.0188	0.0004	0.0066	0.0002	283.4	129.6	126.8	6.4	119.9	2.2	94%
8	121.6026	219.6409	0.5536	0.0508	0.0022	0.1273	0.0061	0.0182	0.0003	0.0058	0.0002	231.6	101.8	121.7	5.5	116.0	2.0	95%
9	334.8453	478.3830	0.7000	0.0500	0.0022	0.1240	0.0055	0.0180	0.0002	0.0055	0.0001	194.5	97.2	118.7	5.0	115.2	1.4	96%
10	340.9971	422.6276	0.8069	0.0471	0.0020	0.1152	0.0048	0.0180	0.0003	0.0054	0.0001	53.8	100.0	110.7	4.4	114.8	1.7	96%
11	233.2171	291.7101	0.7995	0.0503	0.0024	0.1283	0.0062	0.0186	0.0003	0.0058	0.0002	209.3	113.9	122.6	5.5	118.5	1.7	96%
12	298.8906	382.0467	0.7823	0.0492	0.0021	0.1235	0.0055	0.0181	0.0002	0.0057	0.0001	166.8	101.8	118.2	4.9	115.8	1.5	97%
13	132.3046	220.5205	0.6000	0.0500	0.0029	0.1257	0.0068	0.0186	0.0003	0.0061	0.0002	194.5	135.2	120.2	6.1	118.9	1.9	98%
14	296.6256	350.5512	0.8462	0.0475	0.0019	0.1206	0.0049	0.0184	0.0003	0.0060	0.0002	76.0	92.6	115.6	4.4	117.7	1.7	98%
15	706.7336	714.4921	0.9891	0.0475	0.0028	0.1206	0.0073	0.0184	0.0003	0.0059	0.0002	72.3	137.0	115.6	6.6	117.6	1.9	98%
16	1255.4785	1029.4535	1.2196	0.0481	0.0027	0.1241	0.0068	0.0188	0.0003	0.0062	0.0002	105.6	125.9	118.8	6.2	120.0	1.8	98%
17	380.6496	395.3115	0.9629	0.0484	0.0019	0.1215	0.0046	0.0184	0.0003	0.0056	0.0001	120.5	88.0	116.4	4.2	117.5	1.8	99%
18	317.2554	412.9708	0.7682	0.0485	0.0020	0.1221	0.0049	0.0184	0.0002	0.0056	0.0001	124.2	91.7	117.0	4.4	117.6	1.6	99%
19	1232.3453	1087.7727	1.1329	0.0491	0.0033	0.1247	0.0081	0.0187	0.0004	0.0064	0.0003	153.8	151.8	119.4	7.3	119.2	2.2	99%

the dominance of *Pinuspollenites* among a bisaccate conifer pollen.

4.3. *Appendicisporites imperfectus*

4.3.1. *Nomenclature of Appendicisporites imperfectus*

Appendicisporites imperfectus has significant stratigraphic importance, as it serves as a valuable biostratigraphic marker in the palaeobotanical record (Kovaleva et al., 2017). However, some taxonomical issues remain unresolved with respect to taxon nomenclature. *Appendicisporites imperfectus* was first named *Plicatella trichacantha imperfecta* by Malyavkina (1949). It was later reclassified by Bolkhovitina (1961) as *Anemia imperfecta*. Since *Anemia* is not a fossil plant, these fossil fern spores needed a different name. Weyland and Krieger (1953) first proposed it as the genus *Appendicisporites*. This was followed by Pocock (1964), who endorsed the proposal, abandoned the genus *Anemia* and reassigned the taxon to *Appendicisporites*, describing over 15 species from Lower Cretaceous strata in Canada (Pocock, 1964). Until now, most palynologists have considered *Appendicisporites* to be a valid fossil taxon (Pocock, 1964; Kovaleva et al., 2017). However, the potential significance, identification, and usage of *A. imperfectus* are not widely recognized among palynologists due to a lack of detailed descriptions. This study reports the first occurrence of *A. imperfectus* in the Jiufotang Formation and provides comprehensive descriptions to enhance its biostratigraphic relevance and encouraging further research on stratigraphic correlations and palaeoecological interpretation.

4.3.2. *Systematic paleontology*

Order: Filicales.

Family: Lygodiiaceae.

Genus: **Appendicisporites** Weyland and Krieger, 1953.

Type species: *Appendicisporites tricuspidatus* Weyland and Krieger, 1953.

Species: *Appendicisporites imperfectus* Bolchovitina 1961 emend. Ying, Sun et Liang (Figs. 3D; 4A – D).

1949 *Plicicatella trichacantha imperfecta*, Malyavkina, p. 62, pl. 12, fig. 4;

1953 *Appendicisporites imperfecta*, Weyland and Krieger, p. 35, figs. 27, 28;

1961 *Anemia imperfecta*, Bolchovitina, pl. XV, figs. 12a – d; pl. XVII, figs. 1a, b;

2017 *Appendicisporites imperfectus*, Malyavkina, Bolchovitina and Pocock, p. 183, pl. I, fig. 22.

Lectotype: Specimen slide number 423–3–5 (Fig. 3D) is here designated.

Studied Material: One newly collected specimen of *Appendicisporites imperfectus* had been studied. The specimen is deposited in the Key Lab of Evolution of Past Life in NE Asia of Paleontology of Liaoning, Shenyang Normal University, with slide number of 423–3–5.

Locality of the lectotype: Fuxin Basin, Liaoning Province, China.

Stratigraphic horizon: The Jiufotang Formation, Aptian.

(*Emended*) *diagnosis*: Trilete spore with somewhat sinuous suture; length of the rays approximately 3/4 of the radius. Spore outline subcircular to triangular, with a diameter of 66–80 μm. Spore sides straight to slightly convex, with protruding apical angles. In the proximal view, 3–4 sets of rib ornamentations, each set parallel to one side, with approximately 1.0 μm of space between sets, rib widths 5 to 8 μm. In the distal view, 3–6 sets of rib ornamentations, each set also parallel to one side; three joined ribs forming a triangular configuration in the distal pole, additional ribs extending beyond apices of this triangle and irregularly connecting to distal ribs in each set. Adjacent ribs typically connected at their ends, forming three apical corners; the sexine of these three corners thickens and forms three appendices, with heights of 9 μm and widths of 7 μm. Outermost ribs fused at their inflated ends, slight splitting.

Description: The spore exhibits a simple and somewhat sinuous trilete suture with the length of the rays approximately 3/4 of the radius

Table 2
Palynological percentage composition (%) and spectrum (%) from the Jiufotang Formation in the Fuxin Basin.

Sample No. Sporo-pollen	423	422	421	420	419	Palynological spectrum (%)
Spores	1.83	1.65	1.26	1.73	0.43	1.38
Appendicisporites	0.5					0.1
Cyathidites		0.4	0.8			0.24
Lycopodiumsporites				0.4	0.4	0.16
Osmundacidites		0.4	0.4	0.9		0.34
Punctatisporites	1.4	0.8		0.4		0.52
Gymnosperm pollen	98.17	98.35	98.74	98.27	99.57	98.62
Abiespollenites	2.3	2.1	0.4	0.4	2.6	1.56
Abietineaepollenites	1.8	2.1	3.4	4.3	6.4	3.6
Alisporites	4.6	1.7	1.3	3.0	0.9	2.3
Araucariacites	22.5	18.6	23.2	17.3	23.9	21.10
Callialasporites	0.9	0.8	0.4	0.4	0.9	0.68
Cedripites	5.5	4.5	3.0	2.2	3.8	3.80
Chasmatosporites	1.4		0.8	0.9		0.62
Classopollis		2.1	1.68			0.75
Ephedripites		0.4				0.08
Ginkgocycadophytus	4.1	3.3	0.8	0.4	1.3	1.98
Jiaohepollis	1.4	0.8			1.3	0.7
Parcisporites					0.4	0.08
Piceapollenites	12.4	14.9	11.8	13.4	10.3	12.56
Piceites	0.5		0.8			0.26
Pinuspollenites	20.6	22.7	22.8	30.3	26.9	24.66
Podocarpidites	3.2	2.5	0.8	3.0	0.4	1.98
Protopicea	1.4		0.8		0.4	0.52
Protopinus		0.4	0.4	0.4		0.24
Psophosphaera	15.6	21.5	26.2	22.1	20.1	21.10

(Figs. 3D; 4A, B). The outline of the spore is sub-circular to triangular and 66–80 μm in diameter (Fig. 4A – D). The sides are straight to slightly convex, featuring apical angles and protruding corners (Fig. 4A – D). The outermost ribs fuse at their slightly inflated ends, which exhibit slight splitting (Fig. 4A – D). In the proximal view, the ornamentation consists of 3 sets of ribs, each set parallel to 1 side and spaced 0.5–1.0 μm apart, with rib widths ranging from 5 to 8 μm (Fig. 4A, B). In the distal view, the ornamentation comprises 3–6 sets of ribs, which are also parallel to one side (Fig. 4C, D). The distal pole is occupied by an irregular triangular configuration, and the joined ribs in each set show an irregular configuration (Fig. 4C, D). The arrangement of fused ribs on each side forms an inclined comb shape (Fig. 4C). At the apices of the 3 corners, the sexine is thickened to form appendices that measure 9 μm in height and 7 μm in width (Fig. 4C, D).

Comparison: In contrast to the spores of other *Appendicisporites* species, the trilete suture, the size, inflated structure with slightly split appendices and the arrangement of fused ribs on each side exhibit notable differences. When compared to the similar species *A. cooksonii*, the distal sexine ornamented ribs are distinct; compared to *A. laevigatus*, the undulating sexine surface of the latter species differs from that of the present species; furthermore, when compared with other similar species listed in Table 3 (Bolkhovitina, 1961; Pocock, 1964; Pu and Wu, 1985; Singh, 1964; Song et al., 2000).

Remarks: The studied specimen can be classified as *Appendicisporites imperfectus* for several reasons. First, the protruding structure at the corners of the fossil is clearly evident; second, the size of the spore is relatively large, at 66–80 μm in diameter. Third, the irregular arrangement of the joined ribs in each set (Fig. 4C) and the configuration of the fused ribs on each side, which form an inclined comb shape (Fig. 4C, D), are important characteristics of *A. imperfectus*. A typical feature of this species is the outermost ribs fused at their slightly inflated ends, which form appendices that are slightly split.

4.4. Palaeovegetation and palaeoenvironment reconstruction

Spore and pollen fossils originate from terrestrial vegetation, which is highly sensitive to climate and environmental changes (Gao et al., 1999; Deng, 2002, 2007; Wang et al., 2005; Li et al., 2020); therefore, the composition of palynological assemblages responds to these changes (Abbink et al., 2004; Zhao et al., 2014; Li et al., 2020). The ecological environments of the parent plants are categorized following the APJ assemblage and the ecological types (Table 4) of the palynological parent plants from the Jiufotang Formation in the Fuxin Basin (Gao et al., 1999; Abbink et al., 2004; Zhang et al., 2021). Table 5 shows the palynological percentages in relation to vegetation, climate, and humidity types (Gao et al., 1999; Zhao et al., 2014; Zhang et al., 2021). The results demonstrate that the vegetation type in the upper part of the Jiufotang Formation in the Fuxin Basin was predominantly coniferous forest and that the climate was warm temperate with a sub-humid environment.

5. Discussion

5.1. Age of the Jiufotang Formation in the Fuxin Basin

5.1.1. Dating evidence

The Jiufotang Formation represents the third evolutionary stage of the Jehol Biota (Pan et al., 2013; Zhou, 2014; Zhou et al., 2021; Zheng et al., 2023), when it reaches its peak in development and spreads over a large area, the precise age or isotopic dating data remain scarce, and a consensus on the isotopic chronology for this formation has not been reached (He et al., 2004; Chang et al., 2009; Yu et al., 2021). $^{40}Ar/^{39}Ar$ dating of the SHRIMP U–Pb zircon data from the lower part of Jiufotang Formation in the Shangheshou section, Chaoyang City, indicated that the precise age was 120.3 ± 0.7 Ma (He et al., 2004). Chang et al. (2009) reported a $^{40}Ar/^{39}Ar$ age of 122.1 ± 0.3 Ma for a tuff layer from the lowermost Jiufotang Formation near Pijiagou Village of western Liaoning. The latest high-precision geochronological study by Yu et al. (2021) indicates that the Jiufotang Formation in the Jianchang Basin was formed around 122.0–118.9 Ma. Previous radiometric dates were mostly obtained from the tuffs in the middle and lower parts of this formation, while the ages and duration of the upper part tuffs and their equivalent strata related to the late Jehol Biota remain unclear. Our newest LA-ICP-MS zircon U–Pb date for the tuff in the upper part of

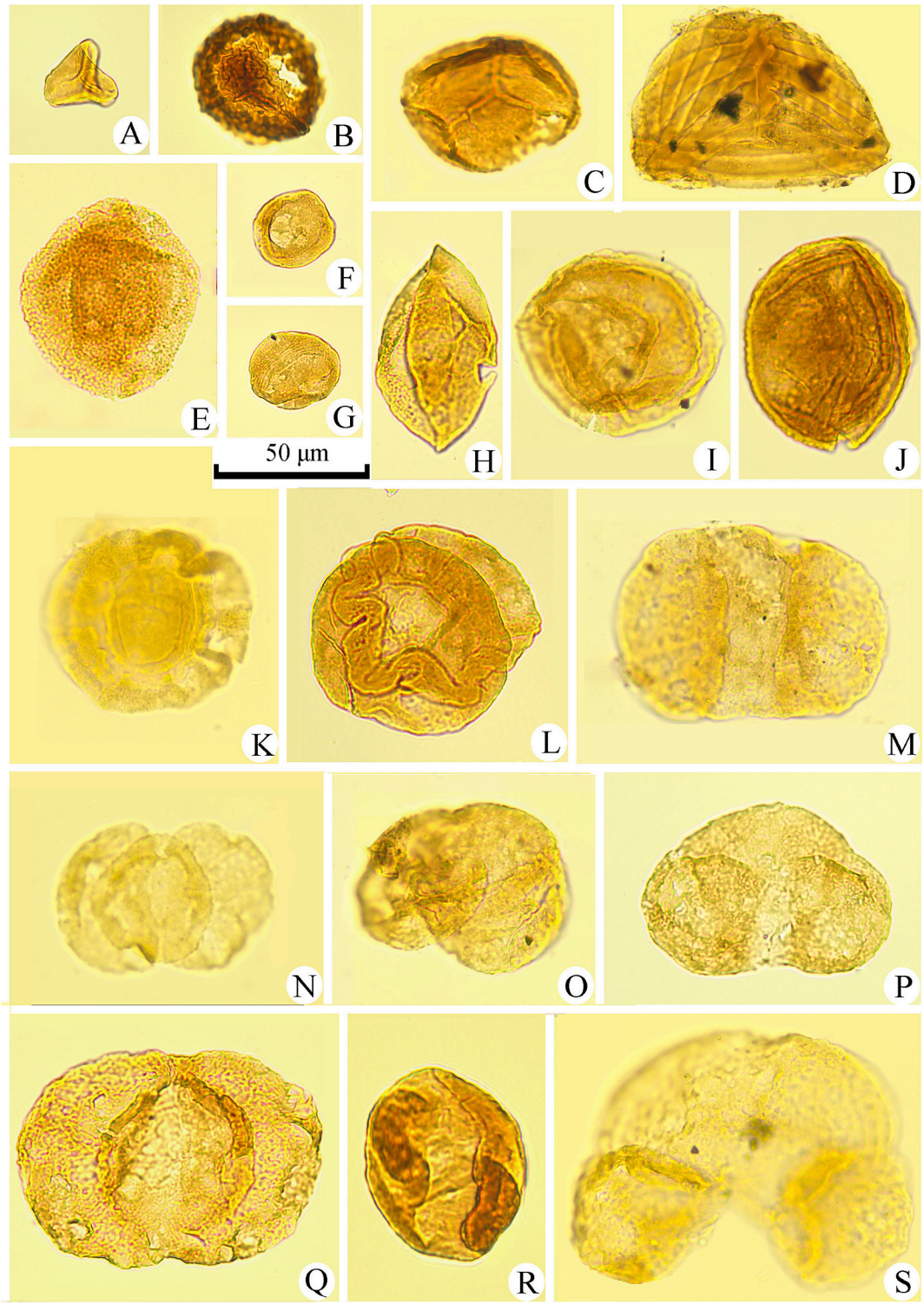

Fig. 3. Fossil spores and pollen from the upper part of the Jiufotang Formation (taxon name is followed by the slide number and position in England finder). A. *Cyathidites minor* Couper, 1953, 422–3–3, O25–4; B. *Lycopodiumsporites* sp., 420–1–4, J12–3; C. *Punctatisporites* sp., 423–2–2, G25–2; D. *Appendicisporites imperfectus* (Maljavkina et Bolchovitina, 1961) Pocock, 1964, 423–3–5, O25–4; E. *Osmundacidites wellmanii* Couper, 1953, 420–2–1, C13–3; F. *Classopollis annulatus* (Verbitzkaja) Li, 1974, 422–2–5, P12–4; G. *Classopollis classoides* Pflug, 1953 emend. Pocock et Jansonius, 1961, 422–4–1, Q22–2; H. *Ginkgocycadophytus* sp., 421–4–2, B24–4; I. *Araucariacites australis* Cookson, 1947, 419–5–1, L17–2; J. *Psophosphaera* sp., 419–5–2, J18–1; K. *Callialasporites dampieri* (Balme, 1957) Sukh Dev, 1961, 421–3–4, K19–4; L. *Jiaohepollis* sp., 419–1–3, F25–3; M. *Alisporites aequalis* Mädler, 1964, 422–3–1, C17–1; N. *Podocarpidites biformis* Rouse, 1957, 420–1–2, H28–2; O. *Cedripites* sp., 419–4–3, D16–2; P. *Piceapollenites complanatiformis* (Bolkh.) Xu et Zhang, 1980, 423–3–4, D15–1; Q. *Piceites* sp., 422–4–1, E20–2; R. *Parcisporites* sp., 423–2–3, E11–4; S. *Pinuspollenites insignis* (Naumova) Pu et Wu, 1982, 420–1–2, K11–1; Scale bar = 50 μm.

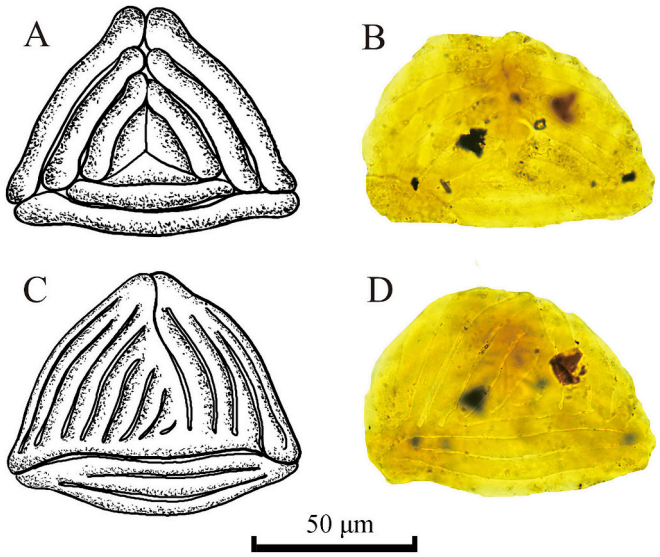

Fig. 4. Sketch diagram of *Appendicisporites imperfectus*.
A. Proximal view picture we drew according to Fig. 3D and Fig. 4B; B. Proximal view of *A. imperfectus* under microscope, slide number 423–3–5; C. Distal view picture we drew according to Fig. 3D and Fig. 4D; D. Distal view under microscope, slide number 423–3–5. Scale bar = 50 μm.

Jiufotang Formation is 118.07 ± 0.9 Ma, providing the youngest age estimates. By combining our new data with previous chronological results, the age of the Jiufotang Formation spans from 122 to 118 Ma, corresponding to the latest Barremian to middle Aptian (He et al., 2004; Chang et al., 2009; Yu et al., 2021; Geologic Time Scale, 2020).

5.1.2. Biostratigraphic correlations

Based on the palynological composition of the APJ assemblage, palynomorphs of significant stratigraphic importance include *Appendicisporites*, *Callialasporites*, and *Jiaohepollis*. Among these, *Appendicisporites* is a key representative of the Cretaceous (Pocock, 1964; Song et al., 2000), with *A. imperfectus* serving as a crucial biostratigraphic element of Aptian palynological assemblages (Weyland and Krieger, 1953; Bolkhovitina, 1961; Kovaleva et al., 2017). *Callialasporites*, commonly found in Jurassic to Early Cretaceous strata (Song et al., 2000), is also present. *Jiaohepollis* was first reported in the Wulin and Naizishan formations, which are now classified as the Changcai Formation, from the Jiaohe Basin of Jilin Province. It is considered a typical index fossil of the Early Cretaceous (Aptian – Albian) period (Li, 1984). These palynomorphs not only signify the stratigraphic importance of the APJ assemblage but also allow for correlations with other notable assemblages. The APJ assemblage has been correlated with the *Piceaepollenites-Cicatricosisporites-Concavissimisporites* and *Concavissimisporites-Heliosporites-Aequitriradites* assemblages of the Jiufotang Formation in the Liaohe and Tieling Basins of western Liaoning Province (Pu and Wu, 1985; Yu et al., 1986), although the two assemblages have a higher abundance of fern spores. This composition difference highlights the distinctiveness of the APJ assemblage. The APJ assemblage also resembles the *Cicatricosisporites-Concavissimisporites-Classopollis* assemblage from the Shen 249 drilling well in the Liaohe Basin (Wen, 2006) and the *Concavissimisporites-Cicatricosisporites-Protoconiferus* assemblage from the Tieling Basin (Wu and Lei, 2007), although it differs in the fern spore content. Many of these palynological assemblages are dominated by gymnosperm pollen, particularly those featuring high bisaccate pollen percentages. Compared with seven palynozones established in the Lower Cretaceous of the South Primorye in Russia, the Aptian palynozone *Rouseisporites laevigatus-Gleicheniidites* is dominated by diverse Gleicheniaceae spores, with a significant number of fern spores with Cyatheaceae and Schizaeaceae affinities (Markevitch, 1994). This composition is distinct from the APJ assemblage. In contrast, the

Table 3
Comparisons with other similar species of *Appendicisporites*.

Species	Size (μm)	Outline	Proximal view	Distal view	Width of ribs (μm)	Appendices structure	References
Appendicisporites imperfectus	66–80	Sub-circular to triangular	Three sets, parallel	3–6 sets, parallel	5–8	Protrude with slightly split	This paper
A. cooksonii	42.0–62.4	Triangular	Parallel	Parallel	5.0	Sharp	Pocock, 1964
A. crickmayii	35	Triangular	Parallel	Three sets, parallel	1.5	Protrude	Pocock, 1964
A. crimensis	43–62	Convex triangular	Three sets, parallel	One set	3–5	Protrude with small spherical	Pocock, 1964
A. cristatus	45.5–50	Triangular	Parallel	Parallel	1.5	Protrude	Pocock, 1964
A. degeneratus	42–63	Triangular	No description	Parallel	3	Protrude	Pocock, 1964
A. erdtmanii	50–55	Triangular	Parallel	Parallel	3.6	Protrude with thickened	Pocock, 1964
A. grandis	60–70	Circular triangular	Three sets, parallel	Parallel	No description	Protrude with thickened	Pocock, 1964
A. irregularis	50–52	Triangular	Three sets, parallel	Three sets, parallel	3.4–4.0	Protrude with thickened	Pocock, 1964
A. macalisteri	65–70	Triangular	Parallel	Parallel	No description	Rounded	Pocock, 1964
A. major	81–115	Triangular	Parallel	Parallel	2.5–5	Protrude	Song et al., 2000
A. perpusillus	28–32	Triangular	Three sets, parallel	Three sets, parallel	1–1.2	Protrude	Pu and Wu, 1985
A. problematicus	45–60	Triangular	Three sets, parallel	Three sets	No description	Protrude	Singh, 1964
A. protensus	48–76	Triangular	Parallel	Parallel	3.5–5	Protrude	Pu and Wu, 1985
A. sellingii	60–66	Triangular	No description	No description	2.5	Sharp	Pocock, 1964
A. spinosus	24.5–33.6	Triangular	Parallel	Parallel	1.0	Sharp	Pocock, 1964
A. singhii	37–45	Triangular	No description	Three sets, parallel	3–4	Protrude with thickened	Pocock, 1964
A. trichacanthus	50–65	Triangular	Three sets, parallel	Parallel	1.8–2.4	Protrude	Pocock, 1964
A. tricostatus	51–80	Triangular	Three sets, parallel	No description	2.5–3.0	Sharp	Pocock, 1964

Table 4
Ecological types of palynological parent plant from the Jiufotang Formation in the Fuxin Basin (according to Gao et al., 1999; Abbink et al., 2004; Zhang et al., 2021).

Sporo-pollen	Vegetation type	Climate type	Humidity type
Fern spores			
Appendicisporites	Shrub	Tropics	Mesophyte
Cyathidites	Evergreen broad-leaf forest	Tropics	Hygrophyte
Lycopodiumsporites	Herb	Tropic-temperate	Hygrophyte
Osmundacidites	Herb	Tropic-temperate	Hygrophyte
Punctatisporites	Herb	Tropic-temperate	Hygrophyte
Gymnosperm pollen			
Abiespollenites	Coniferous forest	Temperate	Mesophyte
Abietineaepollenites	Coniferous forest	Tropic-temperate	Mesophyte
Alisporites	Coniferous forest	Temperate	Mesophyte
Araucariacites	Coniferous forest	Tropics	Hygrophyte
Callialasporites	Coniferous forest	Tropics	Hygrophyte
Cedripites	Coniferous forest	Sub-tropics	Mesophyte
Chasmatosporites	Broad-leaf forest	Tropics-subtropics	Mesophyte
Classopollis	Coniferous forest	Tropics-subtropics	Xerophyte
Ephedripites	Shrub	Temperate	Xerophyte
Ginkgocycadophytus	Evergreen broad-leaf forest	Tropics	Mesophyte
Jiaohepollis	Coniferous forest	Temperate	Mesophyte
Parcisporites	Coniferous forest	Tropics	Hygrophyte
Piceapollenites	Coniferous forest	Temperate	Mesophyte
Piceites	Coniferous forest	Temperate	Hygrophyte
Pinuspollenites	Coniferous forest	Tropic-temperate	Mesophyte
Podocarpidites	Coniferous forest	Tropics	Hygrophyte
Protopicea	Coniferous forest	Temperate	Hygrophyte
Protopinus	Coniferous forest	Temperate	Xerophyte
Psophosphaera	Coniferous forest	Tropic-temperate	Mesophyte

palynological assemblages from the Dongning Formation in the Dongning Basin of China and the Lipovtsy Formation in the adjacent Razdolnaya River Basin of the South Primorye region of Russia all include the typical element *Appendicisporites imperfectus*, which is strictly associated with the Aptian (Malyavkina, 1949; Weyland and Krieger, 1953; Bolkhovitina, 1961; Kovaleva et al., 2017). In summary, the APJ assemblage from the upper part of the Jiufotang Formation in the Fuxin Basin is Aptian. Considering the isotopic data, the age of the Pijiagou section of the Jiufotang Formation has been determined to be middle Aptian.

During the Aptian – Albian of the Early Cretaceous, early angiosperm pollen showed an increasing abundance in coeval Cretaceous palynological assemblages in southern Europe, North America, Brazil, Argentina, and other regions of China (Archangelsky et al., 2009; Heimhofer and Hochuli, 2010; Zhang et al., 2015; Li et al., 2019a, 2019b). However, these fossil records do not comprehensively represent the global angiosperm fossil distribution, since angiosperm pollen from inland continents is relatively scarce (Zhang et al., 2015). This fossil record gap underscores the importance of exploring diverse geological settings.

Volcano-sedimentary and coal-bearing deposits with abundant lacustrine palaeofauna and terrestrial palaeoflora of the Jehol Biota type (Bugdaeva and Golovneva, 2024) are widespread in Transbaikalia (Russia), Mongolia, and northeastern China (Fig. 1A). The sedimentary sequences of these regions are notably similar, as the evolution of the Jehol Biota coincides with the initial and peak stages of North China Craton destruction (Zhou et al., 2021). Active geological processes, particularly volcanism, induced a high level of endemism in the biota, making stratigraphic correlations with adjacent territories straightforward, according to absolute dating. The age of these beds, containing remains of the Jehol Biota, has been considered Barremian to Aptian (Chang et al., 2009, 2012, 2017; He et al., 2004; Smith et al., 1995; Wu et al., 2013; Yang et al., 2020; Yu et al., 2021; Zhong et al., 2021) or Valanginian to Aptian (Li, 2023).

5.2. Palaeoclimate and palaeoenvironment significance

Spores and pollen offer valuable insights into ecological conditions, varied climatic environments, and the paleogeography of their parent plants (Gao et al., 1999; Deng, 2002, 2007; Abbink et al., 2004; Wang et al., 2005; Li et al., 2020). The abundance and diversity of bisaccate pollen from Pinaceae genera, including *Pinuspollenites*, *Cedripites* and *Alisporites*, suggest the presence of high-altitude environments, *Alisporites* is typically associated with coastal areas (Abbink et al., 2004; Wang et al., 2005; Wu and Lei, 2007; Wang et al., 2016; Li et al., 2020). Elevated temperatures during the deposition of the Jiufotang Formation in the Fuxin Basin, may have been influenced by the contemporaneous Cretaceous oceanic anoxic event of the Aptian (OAE1a) (Jenkyns, 2010; Hu et al., 2012; Huber et al., 2018; Jones et al., 2018). The presence of *Classopollis*-bearing conifers suggests the existence of thriving coastal and salt marsh environments (Smith et al., 2024). In contrast, the Cheirolepidiaceae family, which is characterized by *Classopollis* pollen, has adapted to arid regions, saline soils, and swampy lowlands (Alvin, 1982; Krassilov and Bugdaeva, 1982; Deng, 2002, 2007; Smith et al., 2024; Yang et al., 2024).

Ginkgocycadophytus suggests a seasonal palaeoclimate marked by variations that align well with the fossil wood of the Jiufotang Formation (Wang et al., 2015). The climate of the Jiufotang Formation appears to have been more humid and warmer than the Yixian Formation and characterized by seasonal droughts (Pu and Wu, 1985; Li and Liu, 1999; Ding et al., 2003a, 2003b; Ding and Zhang, 2004; Li, 2010; Cui et al., 2015). The mid-Aptian Selenga Formation, Gusinozerskaya Depression, Western Transbaikalia, contains inertinite coals with charcoals (Bugdaeva and Golovneva, 2024). This may indicate a humid climate with drought periods that promoted wildfires. Considering the associated plants, this climate would be more appropriately classified as warm temperate, reflecting varied palynological evidence.

The sedimentary environment of the Jiufotang Formation has a

Table 5
Palynological percentage in vegetation, climate and humidity types of the Jiufotang Formation in the Fuxin Basin (according to Gao et al., 1999; Zhao et al., 2014; Zhang et al., 2021).

		Vegetation types (%)			
Coniferous forest		Broad-leaf forest	Shrub	Herb	Coniferous forest
95.96		2.84	0.17	1.03	
		Climate types (%)			
Tropics	Tropics-subtropics	Sub-tropics	Tropics-temperate	Temperate	Tropics-temperate
26.16	1.38	3.78	50.52	18.16	
		Humidity types (%)			
Xerophyte	Mesophyte	Hygrophyte	Euryphyte	Hydrophyte	Sub-humid
1.12	72.98	25.90	0	0	

Fig. 5. Reconstruction of the Pijiagou section of the Jiufotang Formation in the Fuxin Basin of western Liaoning Province. Drawn by Wen-shuai Wang.

diverse landscape with high mountains, lakes, rivers, and coastal salt marshes (Zhang et al., 2024). These varied environmental settings fostered diverse ecological niches, increasing biodiversity and allowing the late Jehol Biota to flourish (Zhou and Wang, 2017; Xu et al., 2020; Yu et al., 2021). The vertebrate assemblage of the Jiufotang Formation differs significantly from the underlying Yixian Formation (Matsukawa et al., 2014), with terrestrial vertebrate fauna dominated by omnivorous birds. In contrast, herbivorous non-avian dinosaurs dominated the Yixian terrestrial vertebrate fauna (Matsukawa et al., 2014). These changes in the vertebrate fauna from the deposition of the Yixian Formation through the Jiufotang Formation were associated with environmental shifts, as reflected by coniferous forests.

A reconstruction is now possible based on the APJ assemblage and its associated biota in the upper part of the Jiufotang Formation (Fig. 5), including a coniferous forest in low mountains under a sub-humid, warm temperate climate with distinct seasonal changes.

6. Conclusions

(1) The new LA-ICP-MS zircon U–Pb dating (118.07 ± 0.98 Ma) of the rhyolitic tuff from the upper part of the Jiufotang Formation in the Fuxin Basin indicates an age in the middle Aptian.
(2) The *Appendicisporites-Pinuspollenites-Jiaohepollis* assemblage of the Jiufotang Formation in the Pijiagou section of the Fuxin Basin, including the new occurrence of *Appendicisporites imperfectus*, is recognized as a valid biostratigraphic indicator of the Aptian that provides significant palynological evidence for dating.
(3) The palynological assemblage indicates coniferous forests on hilled mountains near a marine shoreline under a sub-humid, warm-temperate climate with distinct seasonal changes.

Declaration of competing interest

The authors declare that they have no conflict of interest.

Data availability

No data was used for the research described in the article.

Acknowledgements

The research was supported by China Geological Survey projects (Grant No. DD20242686) and the National Natural Science Foundation of China (42172017) and the Fundamental Research Funds for the Liaoning Universities (SYNUXJ2024049, LJ202410166029), and the Scientific Research Foundation of Shenyang Normal University (BS202305). The research of E.V. Bugdaeva was carried out within the state assignment of Ministry of Science and Higher Education of the Russian Federation (No. 124012200182-1). Heartfelt thanks to Professor Abdul Rahman Ashraf of Bonn University, for his help with palynomorph identification and laboratory procedures. Many thanks to Wen-shuai Wang for the reconstruction picture of Fig. 5 and to students of Paleontology College of Shenyang Normal University for their assistance in the field, as well as to the editor and anonymous reviewers for their kind comments on the manuscript. We thank LetPub (www.letpub.com.cn) for its linguistic assistance during the preparation of this manuscript.

References

Abbink, O.A., Van Konijnenburg-Van Cittert, J.H.A., Visscher, H., 2004. A sporomorph ecogroup model for the Northwest European Jurassic–Lower Cretaceous I: concepts and framework. Netherl. J. Geosci. Mijnbouw 83, 17–38.
Alvin, K.L., 1982. Cheirolepidiaceae: Biology, structure and paleoecology. Rev. Palaeobot. and Palynolo. 37, 71–98.
Archangelsky, S., Barreda, V., Passalia, M.G., Gandolfo, M., Prámparo, M., Romero, E., Cúneo, R., Zamuner, A., Iglesias, A., Llorens, M., Puebla, G.G., Quattrocchio, M., Volkheimer, W., 2009. Early angiosperm diversification: evidence from southern South America. Cretaceous Res. 30, 1073–1082.
Bolkhovitina, N.A., 1961. Fossil and Recent Spores of Family Schizaeaceae. Academy of Sciences of USSR Publishing House, Moscow, pp. 176 (in Russian).
Bugdaeva, E.V., Golovneva, L.B., 2024. Siberian Jehol Biota. In: Hart, M.B., Batenburg, S. J., Huber, B.T., Price, G.D., Thibault, N., Wagreich, M., Walaszczyk, I. (Eds.), Cretaceous Project 200. Volume 2: Regional Studies. Geological Society, London, Special Publications, London, p. 545.
Chang, S.C., Zhang, H.C., Renne, P.R., Fang, Y., 2009. High-precision $^{40}Ar/^{39}Ar$ age for the Jehol Biota. Palaeogeogr. Palaeoclimatol. Palaeoecol. 280, 94–104.
Chang, S.C., Zhang, H.C., Hemming, S.R., Mesko, G.T., Fang, Y., 2012. Chronological evidence for extension of the Jehol Biota into Southern China. Palaeogeogr. Palaeoclimatol. Palaeoecol. 344 – 345, 1–5.
Chang, S.C., Gao, K.Q., Zhou, C.F., Jourdan, F., 2017. New chronostratigraphic constraints on the Yixian Formation with implications for the Jehol Biota. Palaeogeogr. Palaeoclimatol. Palaeoecol. 487, 399–406.
Chen, P.J., Jin, F., 1999. Jehol Biota (in Chinese). University of Science and Technology of China Press, Hefei, pp. 1–342.

Chen, G., Zhang, X.M., Yang, G.F., Han, G., Bian, J., Yang, Y.N., Zhuo, S.G., 2019. Sedimentary and organic matter characteristics of Lower Cretaceous Jiufotang Formation in western Liaoning Province. Geol. Bull. China 38 (2/3), 426–436.
Cui, Y., Gong, E.P., Wang, T.H., Guan, C.Q., Zhang, Y.L., Liang, J.H., 2015. Palynomorph assemblages and paleoclimate records from the Zhuanchengzi Bed of the Yixian Formation western Liaoning Province, China. Sci. China Earth Sci. 58, 1538–1552 (in Chinese).
Deng, S.H., 2002. Ecology of the Early Cretaceous ferns of Northeast China. Rev. Palaeobot. Palynol. 119, 93–112.
Deng, S.H., 2007. Palaeoclimatic implications of main fossil plants of the Mesozoic. J. Palaeogeogr. 9 (6), 559–574 (in Chinese with English abstract).
Ding, Q.H., Zhang, L.D., 2004. Spore-pollen flora as the indicator of paleoclimate condition in the Yixian Formation, western Liaoning Province. Acta Micropalaeontol. Sin. 21 (3), 332–341 (in Chinese with English abstract).
Ding, Q.H., Zhang, L.D., Guo, S.Z., Zhang, C.J., Peng, Y.D., Jia, B., Chen, S.W., Xing, D.H., 2003a. Palaeoclimatic and palaeoenvironmental proxies of the Yixian Formation in the Beipiao area, western Liaoning. Geol. Bull. China 22 (3), 186–191 (in Chinese with English abstract).
Ding, Q.H., Zhang, L.D., Guo, S.Z., Zhang, C.J., Peng, Y.D., Jia, B., Chen, S.W., Xing, D.H., 2003b. Study on the paleoecology of Yixian Formation in Beipiao area, western Liaoning Province, China. J. Precious Metal. Geol. 12 (1), 9–18 (in Chinese with English abstract).
Gao, R.Q., Zhao, C.B., Qiao, X.Y., Zheng, Y.L., Yan, F.Y., Wan, C.B., 1999. Cretaceous Oil Strata Palynology from Songliao Basin. Geological Publishing House, Beijing, pp. 1–373 (in Chinese with English abstract).
Geng, J.Z., Li, H.K., Zhang, J., Zhou, H.Y., Li, H.M., 2011. Zircon Hf isotope analysis by means of LA-MC-ICP-MS. Geol. Bull. China 30 (10), 1508–1513.
Geologic Time Scale, 2020. In: Gradstein, F.M., Ogg, J.G., Schmitz, M.D., Ogg, G.M. (Eds.), 2020. (2 vols). Elsevier, Amsterdam. Oxford, Cambridge, pp. 1357.
He, H.Y., Wang, X.L., Zhou, Z.H., Wang, F., Boven, A., Shi, G.H., Zhu, R.X., 2004. Timing of the Jiufotang Formation (late Jehol Group) in Liaoning, northeastern China, and its implications. Geophys. Res. Lett. 31, L12605.
Heimhofer, U., Hochuli, P.A., 2010. Early Cretaceous angiosperm pollen from a low latitude succession (Araripe Basin, NE Brazil). Rev. Palaeobot. Palynol. 161, 105–126.
Hou, K.J., Li, Y.H., Tian, Y.R., 2009. *In situ* U-Pb zircon dating using laser ablation-multi ion counting ICP-MS. Miner. Deposit 28 (4), 481–492.
Hu, X., Wagreich, M., Yilmaz, I.O., 2012. Marine rapid environmental/climatic change in the Cretaceous greenhouse world. Cretac. Res. 38, 1–6.
Huber, B.T., MacLeod, K.G., Watkins, D.K., Coffin, M.F., 2018. The rise and fall of the Cretaceous Hot Greenhouse climate. Global Planet. Change 167, 1–23.
Jackson, S.E., Pearson, N.J., Griffin, W.L., Belousova, E.A., 2004. The application of laser ablation-inductively coupled plasma-mass spectrometry (LA-ICP-MS) to in situ U-Pb zircon geochronology. Chem. Geol. 211, 47–69.
Jenkyns, H.C., 2010. Geochemistry of oceanic anoxic events. Geochem. Geophys. Geosyst. 11 (3), 1–30.
Ji, Q., Chen, W., Wang, W.L., Jin, X.C., Zhang, J.P., Liu, Y.Q., Zhang, H., Yao, P.Y., Ji, S. A., Yuan, C.X., Zhang, Y., You, H.L., 2004. Mesozoic Jehol Biota of Western Liaoning, China (in Chinese). Geological Publishing House, Beijing, p. 375.
Jones, M.M., Ibarra, D.E., Gao, Y., Sageman, B.B., Selby, D., Chamberlain, C.P., Graham, S.A., 2018. Evaluating Late Cretaceous OAEs and the influence of marine incursions on organic carbon burial in an expansive East Asian paleo-lake. Earth Planet. Sci. Lett. 484, 41–52.
Koschek, G., 1993. Origin and significance of the SEM cathodoluminescence from zircon. J. Microsc. 171 (3), 223–232.
Kovaleva, T.A., Markevich, V.S., Sun, G., 2017. Age and Palynological Characteristic of the Dongning Formation (Eastern Heilongjiang, China). Tikhookeanskaya Geologiya, Russ. J. Pacific Geol. 11 (3), 178–190.
Krassilov, V.A., Bugdaeva, E.V., 1982. Achene-like fossils from the Lower Cretaceous of the Lake Baikal area. Rev. Palaeobot. Palynol. 36, 279–295.
Li, W.B., 1984. Palynology of Early Cretaceous of Jiaohe Basin, Jilin Province. Proc. Nanjing Inst. Geol. Palaeontol. Chin. Acad. Sci. 1984 (19), 67–141.
Li, W.B., 2010. Palynological assemblage from the Zhuanchengzi beds of Yixian Formation in Jinjiagou, Yixian. Acta Palaeontol. Sin. 49 (1), 44–53 (in Chinese with English abstract).
Li, G., 2023. New spinicaudatan species (Crustacea) of the Lower Cretaceous (Valanginian–Hauterivian) Jehol Biota from northern Hebei, China. Cretac. Res. 143, 105425.
Li, W.B., Liu, Z.S., 1999. Sporomorph assemblage from the basal Yixian Formation in western Liaoning and its geological age. Palaeoworld 11, 68–79 (in Chinese with English summary).
Li, J.G., Sha, J.G., McLoughlin, S., Wang, X.M., 2019a. Mesozoic and Cenozoic palaeogeography, palaeoclimate and palaeoecology in the eastern Tethys. Palaeogeogr. Palaeoclimatol. Palaeoecol. 515, 1–5.
Li, J.G., Wu, Y.X., Peng, J.G., Batten, D.J., 2019b. Palynofloral evolution on the northern margin of the Indian Plate, southern Xizang, China during the Cretaceous Period and its phytogeographic significance. Palaeogeogr. Palaeoclimatol. Palaeoecol. 515, 107–122.
Li, L.Q., Wang, Y.D., Kürschner, W.M., Ruhl, M., Vajda, V., 2020. Palaeovegetation and palaeoclimate changes across the Triassic–Jurassic transition in the Sichuan Basin, China. Palaeogeogr. Palaeoclimatol. Palaeoecol. 556, 109891.
Liu, Y.S., Hu, Z.C., Gao, S., Günther, D., Xu, J., Gao, C.G., Chen, H.H., 2008. In situ analysis of major and trace elements of anhydrous minerals by LA-ICP-MS without applying an internal standard. Chem. Geol. 257, 34–43.
Liu, Y.S., Gao, S., Hu, Z.C., Gao, C.G., Zong, K.Q., Wang, D.B., 2010. Continental and oceanic crust recycling-induced melt-peridotite interactions in the Trans-North China Orogen: U-Pb dating, Hf isotopes and trace elements in zircons from mantle xenoliths. J. Petrol. 51, 537–571.
Ludwig, K.R., 2003. Isoplot 3.0: a geochronological toolkit for Microsoft Excel. In: Berkeley Geochronol Center Special Publications, pp. 1–70.
Malyavkina, V.S., 1949. Key to Spores and Pollen. Jurassic–Cretaceous. Gostoptekhizdat Publishing House, Leningrad–Moscow, pp. 138 (in Russian).
Markevitch, V.S., 1994. Palynological zonation of the continental Cretaceous and lower Tertiary of eastern Russia. Cretac. Res. 15 (2), 165–177.
Matsukawa, M., Shibata, K., Sato, K., Xu, X., Lockley, M.G., 2014. The Early Cretaceous terrestrial ecosystems of the Jehol Biota based on foodweb and energyflow models. Biol. J. Linn. Soc. 113, 836–853.
Pan, Y.H., Sha, J.G., Zhou, Z.H., Fürsich, F.T., 2013. The Jehol Biota: Definition and distribution of exceptionally preserved relicts of a continental Early Cretaceous ecosystem. Cretac. Res. 44, 30–38.
Pocock, S.A.J., 1964. Pollen and spores of the Chlamydospermidae and Schizaeaceae from Upper Mannville Strata of the Saskatoon Area of Saskatchewan. Grana 5 (2), 129–209.
Pu, R.G., Wu, H.Z., 1985. Mesozoic Sporo-Pollen Assemblages in Western Liaoning and their Stratigraphic Significance. Mesozoic Stratigraphy and Paleontology in Western Liaoning (2). Geology Publishing House, Beijing, pp. 121–212.
Sha, J., 2007. Cretaceous stratigraphy of Northeast China: non-marine and marine correlation. Cretac. Res. 28, 146–170.
Singh, H.P., 1964. Microflora of the Lower Cretaceous Mannville Group, east-central Alberta. Res. Alberta Bull. 15, 1–238.
Smith, P.E., Evensen, N.M., York, D., Chang, M.M., Jin, F., Li, J.L., Cumbaa, S., Russel, D., 1995. Dates and rates in ancient lakes: ^{40}Ar-^{39}Ar evidence for an Early Cretaceous age for the Jehol Group, Northeast China. Can. J. Earth Sci. 32, 1426–1431.
Smith, V., Hessler, A., Moscardelli, L., Bord, D., Olariu, J., Lorente, M.A., Sivil, E., Liu, X. J., 2024. A late refugium for *Classopollis* in the Paleocene Lower Wilcox Group along the Texas Gulf Coast. Geology 52, 251–255.
Song, Z.C., Shang, Y.K., Liu, Z.S., Huang, P., Wang, X.P., Qian, L.J., Du, B.A., Zhang, D. H., 2000. Fossil spores and pollen of China. In: The Mesozoic Spores and Pollen, vol. 2. Science Press, Beijing, pp. 1–710.
Su, Y.S., Gao, J.H., Li, S.J., Bu, C.P., Zhu, C.Q., 2008. The basin growth characteristic and hydrocarbon assessment of the Mesozoic in Songnan–Liaoxi Area. Geoscience 22 (4), 505–511.
Wan, X.Q., Chen, P.J., Wei, M.J., 2007. The Cretaceous system in China. Acta Geol. Sin. 81, 957–983.
Wang, W.F., Lu, S.G., Xie, X.Y., Sun, Y.P., 1998. Tectonic geometory and type of traps in Fuxin Basin. J. Univ. Petrol. China 22 (3), 26–30.
Wang, Y.D., Mosbrugger, V., Zhang, H., 2005. Early to Middle Jurassic vegetation and climatic events in the Qaidam Basin, Northwest China. Palaeogeogr. Palaeoclimatol. Palaeoecol. 224, 200–216.
Wang, X.Q., Tian, N., Wang, Y.D., Zhu, Z.P., Li, Y.L., 2015. Discovery of petrified wood from Lower Cretaceous Jiufotang Formation in Yixian of western Liaoning, NE China and its significance. Global Geol. 34 (4), 879–885.
Wang, D.N., Wang, X.R., Ji, Q., 2016. The palynoflora alternation and the paleoclimate change at the turning time between Late Jurassic and Early Cretaceous in Northern Hebei and Western Liaoning. Acta Geosci. Sin. 37 (4), 449–459.
Wang, X.R., Huang, J.D., Martin, K., Andrea, C., Liu, X.Y., Wang, Y., Ju, S.B., 2020. A new *jeholornithiform* exhibits the earliest appearance of the fused sternum and pelvis in the evolution of avialan dinosaurs. J. Asian Earth Sci. 199, 104401.
Wen, G.Q., 2006. Early Cretaceous Jiufotang Formation Palynological assemblage in Shen 249 wells, Damentun Depression, Liaohe Basin. Acta Micropalaeontol. Sin. 23 (2), 191–198.
Wu, B.W., Lei, A.G., 2007. Early Cretaceous Palynological assemblages in Tieling Basin, Liaoning. Acta Micropalaeontol. Sin. 24 (1), 89–97.
Wu, H.C., Zhang, S.H., Jiang, G.Q., Yang, T.S., Guo, J.H., Li, H.Y., 2013. Astrochronology for the Early Cretaceous Jehol Biota in northeastern China. Palaeogeogr. Palaeoclimatol. Palaeoecol. 385, 221–228.
Wu, B.W., Guo, Y.M., Wang, X., Wang, X., Jiang, L., Wang, H., Ji, Z.K., 2015. The oil-gas exploration direction of Fuxin Basin. Geol. Resour. 24 (5), 473–477.
Wu, Z.J., Gao, F.L., Pan, Y.Q., Wang, X., 2018. Division and correlation of the Jiufotang Formation and their rare fossil-bearing beds in Western Liaoning, China. Geoscience 32 (4), 758–765.
Weyland, H., Krieger, W., 1953. Die Sporen und Pollen der aachener Kreide und ihre Bedeutung für die Charakterisierung des mittleren Senons. Palaeontogr. Abt. B, 95, Lief. 1 – 3, 2–29.
Xi, D.P., Wan, X.Q., Li, G.B., Li, G., 2019. Cretaceous integrative stratigraphy and timescale of China. Sci. China Earth Sci. 62, 256–286.
Xu, X., Zhou, Z., Wang, Y., Wang, M., 2020. Study on the Jehol Biota: recent advances and future prospects. Sci. China Earth Sci. 63, 757–773.
Yang, S.H., He, H.Y., Jin, F., Zhang, F.C., Wu, Y.B., Yu, Z.Q., Li, Q.L., Wang, M., O'Connor, J.M.K., Deng, C.L., Zhu, R.X., Zhou, Z.H., 2020. The appearance and duration of the Jehol Biota: constraint from SIMS U-Pb zircon dating for the Huajiying Formation in northern China. Proc. Natl. Acad. Sci. U. S. A. 117, 14299–14305.
Yang, Q., Ying, Q.E., Li, L.Q., Zhang, J., Gong, F.H., Sun, S.L., Wang, H.S., Tan, X., Liang, F., 2024. Palynological evidence for the Late Cretaceous lake transgression event in the Songliao Basin, NE China. Cretac. Res. 165, 105971.
Yu, J.X., Pu, R.G., Wu, H.Z., 1986. Sporo-pollen assemblages from the upper part of the Rehe Group, Liaoning Province. Bull. Chin. Acad. Geol. Sci. 13, 93–107. Geological Publishing House. (in Chinese).
Yu, Z.Q., Wang, M., Li, Y.J., Deng, C.L., He, H.Y., 2021. New geochronological constraints for the Lower Cretaceous Jiufotang Formation in Jianchang Basin, NE

China, and their implications for the late Jehol Biota. Palaeogeogr. Palaeoclimatol. Palaeoecol. 583, 110657.
Zhang, H., Liu, X.M., Li, Z.T., Yang, F.L., Wang, X.R., 2005. Early Cretaceous large-scale crustal thinning in the Fuxin－Yixian Basin and adjacent area in western Liaoning. Geol. Rev. 51 (4), 360–372.
Zhang, L.J., Yang, Y.J., Zhang, L.D., Guo, S.Z., Wang, W.L., Zheng, S.L., 2007. Precious Fossil-Bearing Beds of the Lower Cretaceous Jiufotang Formation in Western Liaoning Province, China. Acta Geol. Sin. 81 (3), 357–364.
Zhang, M.Z., Ji, L.M., Du, B.X., Dai, S., Hou, X.W., 2015. Palynology of the Early Cretaceous Hanxia Section in the Jiuquan Basin, Northwest China: the discovery of diverse early angiosperm pollen and paleoclimatic significance. Palaeogeogr. Palaeoclimatol. Palaeoecol. 440, 297–306.
Zhang, J.G., Lenz, O.K., Wang, P.J., Hornung, J., 2021. The Eco-Plant model and its implication on Mesozoic dispersed sporomorphs for Bryophytes, Pteridophytes, and Gymnosperms. Rev. Palaeobot. Palynol. 293, 104503.
Zhang, L.J., Ji, S.A., Zhang, H.C., 2024. Discovery of the choristodere *Hyphalosaurus baitaigouensis* from the Lower Cretaceous Jiufotang Formation of western Liaoning, China and its paleobiogeographic significance. J. Palaeogeogr. 13, 547–562.
Zhao, J., Wan, X.Q., Xi, D.P., Jing, X., Li, W., Huang, Q.H., Zhang, J.Y., 2014. Late Cretaceous palynology and paleoclimate change: evidence from the SK1 (South) core, Songliao Basin, NE China. Sci. China Earth Sci. 57, 2985–2997.
Zheng, D.R., Chang, S.C., Ramezani, J., Xu, X., Xu, H.H., Wang, H., Pei, R., Fang, Y.N., Wang, J., Wang, B., Zhang, H.C., 2023. Calibrating the Early Cretaceous Urho Pterosaur Fauna in Junggar Basin and implications for the evolution of the Jehol Biota. Geol. Soc. Am. Bull. 136 (2), 765–773.
Zhong, Y.T., Huyskens, M.H., Yin, Q.Z., Wang, Y.Q., Ma, Q., Xu, Y.G., 2021. High-precision geochronological constraints on the duration of 'Dinosaur Pompeii' and the Yixian Formation. Natl. Sci. Rev. 8, nwab063.
Zhou, Z.H., 2014. The Jehol Biota, an Early Cretaceous terrestrial Lagerstätte: new discoveries and implications. Natl. Sci. Rev. 1, 543–559.
Zhou, Z.H., Wang, Y., 2017. Vertebrate assemblages of the Jurassic Yanliao Biota and the Early Cretaceous Jehol Biota: comparisons and implications. Palaeoworld 26, 241–252.
Zhou, Z.H., Barrett, P.M., Hilton, J., 2003. An exceptionally preserved Lower Cretaceous ecosystem. Nature 421, 807–814.
Zhou, Z.H., Meng, Q.R., Zhu, R.X., Wang, M., 2021. Spatiotemporal evolution of the Jehol Biota: responses to the North China craton destruction in the Early Cretaceous. Proc. Natl. Acad. Sci. U. S. A. 118, e2107859118.